

A Temperature-Dependent Multi-Rate Robust Controller for Hard Disk Drives

Keitaro OHNO* and Shinji HARA*

This paper is concerned with practical ways of design and implementation of an \mathcal{H}_∞ controller for hard disk drives (HDDs). In spite of its efficiency in terms of systematic design capability, the \mathcal{H}_∞ method is not thoroughly introduced in HDD industry. The reasons are thought to include 1) difficulties on the measure to the changes of mechanical resonant characteristics by temperature fluctuation that tend to make the \mathcal{H}_∞ controller conservative, 2) considerations on a computational saving multi-rate implementation, 3) difficulties on maintaining the controller after design. A temperature dependent uncertainty model for a standard continuous-time \mathcal{H}_∞ design, and a frequency division technique for re-design of the resultant controller with multi-rate and temperature-dependent implementation, are proposed as keys to overcome to those problems. The effectiveness is confirmed by several experiments as well as simulations which show that the proposed controller can improve the positioning accuracy compared to the standard multi-rate controller.

Key Words: hard disk drives, multi-rate control, temperature-dependence, robust control

1. Introduction

One of the limiting factors to the servo performance of hard disk drive (HDD) head positioning systems is the existence of several mechanical resonant modes in actuators. These resonant modes must be compensated by a filter with sufficiently wide and deep frequency characteristics in order to guarantee the robust stability, while the compensation deteriorates the positioning accuracy. Consequently, it is requisite to balance two contradictory issues with careful considerations on exogenous disturbances and model uncertainties.

This naturally leads the HDDs industry to introduce \mathcal{H}_∞ based control design^{1)~5)}. However, in spite of their efforts and the efficiency of the design method in terms of systematic design capability, the \mathcal{H}_∞ method is not thoroughly introduced in HDD industry. The reasons are thought to include 1) difficulties on the measure to the changes of mechanical resonant characteristics by temperature fluctuation that tend to make the \mathcal{H}_∞ controller conservative, 2) considerations on a computational saving multi-rate implementation, 3) difficulties on maintaining the controller after design.

Our first proposal toward those problems is about how to deal with the temperature fluctuation. Some commercial drives have 5% variation in resonant frequency,

while the total variation including the unit-to-unit variation is around 10%. In this paper, we propose to separate such a temperature-originated uncertainty from total one by obtaining a simple temperature dependent uncertainty model (TDUM).

Our second proposal is a technique that we call frequency division technique (FDT), and it is related to two issues. One is how to re-design the resultant \mathcal{H}_∞ controller as temperature dependent filter, and another one is about the multi-rate implementation that reduce the computational cost in practice. The FDT is based on the following observation. The filter to be temperature dependent may be decoupled from other parts. Also it dominates the fast modes since it treats the resonant modes in the higher frequency range while other parts dominate the slow modes. The slow modes may be operated in a rather slow sampling frequency while the fast modes should be operated in a sufficiently fast sampling frequency⁶⁾.

The two proposals above also contribute to the maintenance capability since most of its difficulties come from the measures to the changes of the resonant characteristics after \mathcal{H}_∞ design. In our proposed controller, we can just re-design the high-rate filter instead of following all the \mathcal{H}_∞ procedure.

Our design procedure is as follows. First, we obtain a TDUM based on the frequency responses. We apply a standard continuous-time \mathcal{H}_∞ control design with D -scaling. Secondly, we divide the resultant \mathcal{H}_∞ controller into a series of several filters depending on the frequencies of its poles and zeros, so that we can use a part of them

* Department of Information Physics and Computing, Graduate School of Information Science and Engineering, University of Tokyo, Tokyo 113-8656, Japan.
(Received February 10, 2006)

as a notch-type filter. Thirdly, we modify the notch-type filter as a function of temperature by using a TDUM. Finally, we apply an up-sampler to the notch-type filter. Our final multi-rate digital controller consists of a low-rate fixed controller and a high-rate temperature dependent notch-type filter. With this configuration, we can obtain an efficient temperature dependent controller with computational saving multi-rate implementation.

The effectiveness will be confirmed by both simulations and experiments, which show that the proposed controller can improve the positioning accuracy compared to conventional standard multi-rate controller.

This paper is organized as follows. We first describe a way of uncertainty modeling of HDDs and clarify the temperature dependency and obtain a TDUM in Section 2. Section 3 is devoted to the \mathcal{H}_∞ control design with D -scaling followed by controller order reduction by a least square fitting. In Section 4, we first explain the basic idea of the FDT, and then provide a practical design of a computational-saving temperature-dependent robust controller. The resultant controller is evaluated through experiments as well as a set of simulations to confirm the effectiveness of our proposed scheme in Section 5.

2. Modeling a target HDD

The positioning mechanism of HDDs⁷⁾ consists of magnetic disks, magnetic heads, arms, and a voice coil motor (VCM) as illustrated in Fig. 1. Position data is embedded on the disk itself whose area is called servo frame, and they are aligned between sectors like the spokes of a wheel. The measurement signal or the position error signal (PES) can be obtained when the head crosses the servo frame.

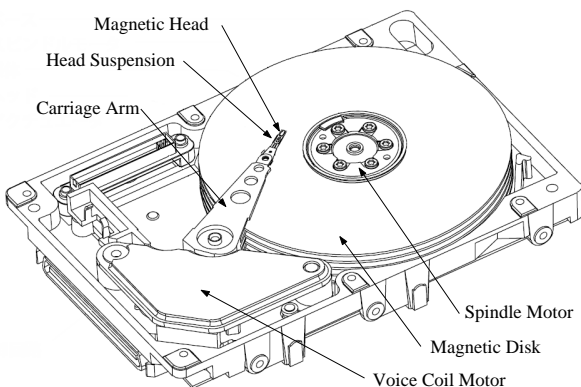


Fig. 1 Hard disk drive

Our goal is to improve the positioning accuracy during

the track-following operation. This requires the disturbance rejection performance to be optimized. Thus, careful investigation on estimating the disturbances is requisite. Fig. 2 shows the mean spectrum of the estimated disturbances of a target drive with 7,200rpm and 11kHz sampling, which is calculated from the PES for several different positions for all the heads of several different hard disk units. Notice that all the exogenous disturbances are assumed to be additively input in the plant output as implied in this figure.

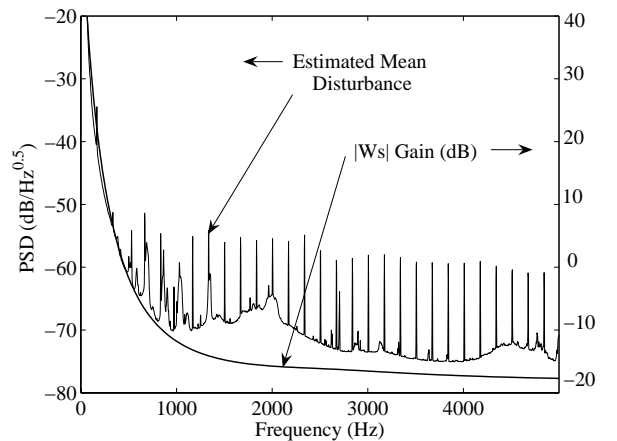


Fig. 2 Estimated mean disturbance spectrum and weighting function W_s for \mathcal{H}_∞ design

The head suspension system including the arms, the magnetic heads, and the VCM normally has two to three resonant modes at around 5 to 8kHz⁸⁾. Our case is not the exception as we can see from the measured frequency response of the plant in Fig. 3. Experimental data are obtained by using 15 different units at two different tracks each (inner/outer of the disk) with two different heads each under 13 different temperature conditions ranging from 0 to 60 degree-C. The nominal model is obtained by applying a standard curve fit method to an averaged frequency response as follows.

$$P(s) = k \left(\frac{1}{s^2} + \sum_{i=1}^2 \frac{r_i}{s^2 + 2\zeta_i \omega_i s + \omega_i^2} \right) e^{-T_d s}, \quad (1)$$

where k is a constant gain, and ζ_i , r_i , and ω_i are i -th mode damping factor, residue, and resonant frequency, respectively. The time delay, denoted by T_d , includes the effect of delay caused by zero-order hold (ZOH), which is half of the sampling period. We approximate the time delay factor $e^{-T_d s}$ by a second order transfer function by using Padé approximation⁹⁾ as follows:

$$e^{-T_d s} \simeq \frac{(s^2 - 6.818 \times 10^4 s + 1.55 \times 10^9)}{(s^2 + 6.818 \times 10^4 s + 1.55 \times 10^9)}, \quad (2)$$

where $T_d = 88\mu s$.

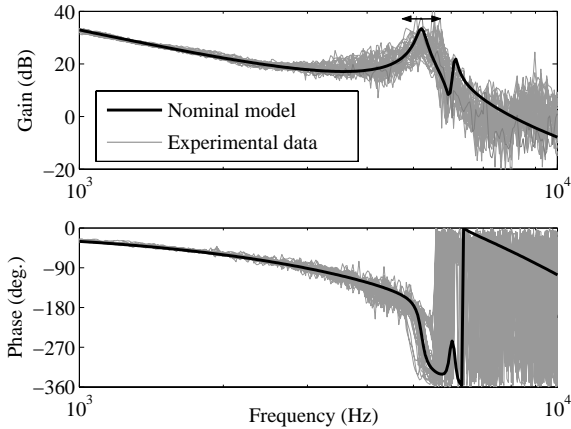


Fig. 3 Measured plant frequency responses and its nominal model

Table 1 shows the nominal plant parameters. These parameters are identified from the results in Fig. 3. Each parameter has a certain level of perturbation, but what is remarkable is the perturbation for the first mode resonant frequency ω_1 as illustrated in Fig. 3. The perturbation level reaches up to 10%, and is the primary cause to hinder boosting up the servo bandwidth. However, when the temperature is maintained, the perturbation level is reduced by half from 10% to 5% as is shown in **Table 2**.

Table 1 Nominal plant parameters

F_s	Sampling frequency	11kHz
ω_1	1 st resonant frequency	5200Hz
ω_2	2 nd resonant frequency	6100Hz
ζ_1	1 st resonant damping factor	0.02
ζ_2	2 nd resonant damping factor	0.01
r_1	Residue of 1 st resonant mode	-1.2
r_2	Residue of 2 nd resonant mode	-0.2
k	Constant gain	1.3×10^8
T_d	Time delay including ZOH effect	88 μs

Table 2 Perturbation of first mode resonant frequency

Temperature range (degree-C)	Perturbation level (%)
0 ~ 60	10
maintained within ± 1	5

Now, let us discuss the TDUM. A lot of dotted lines in **Fig. 4** are the multiplicative errors of the plant when the temperature is maintained, and the bold solid line is the maximum perturbation which covers all these dotted lines. On the other hand, the maximum perturbation

model for the case when the temperature is not maintained is depicted as a thin solid line. By comparing these two maximum perturbation models, we can see how much conservativeness in the design is reduced by considering the temperature dependency. Moreover, the relation between the resonant frequency and the temperature is parameterized as

$$\omega_1 = -10 \cdot T_w + 5500, \quad (3)$$

where T_w is the disk enclosure temperature. The effectiveness of using the TDUM will be discussed in Section 4 and confirmed by simulations as well as experiments in Section 5. Notice that, from the authors experiences, although the temperature dependence of almost all the HDD models can be parameterized as a linear function as in (3), it does not necessarily have to be linear and any kind of function can be dealt with by the proposed method if it is implementable on the on-board MPU/DSP.

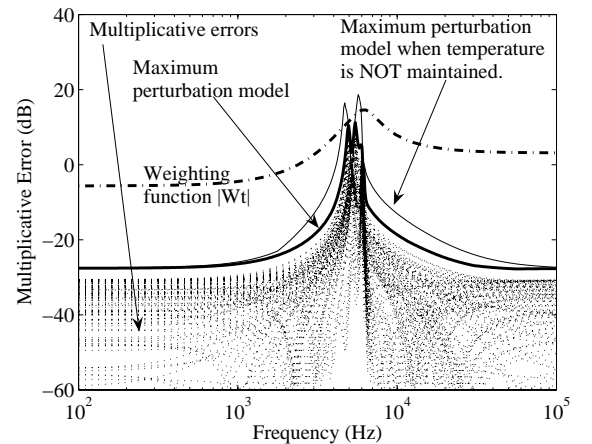


Fig. 4 Multiplicative error of the plant, maximum perturbation model, and weighting function Wt for \mathcal{H}_∞ design

3. \mathcal{H}_∞ control design with D -scaling

In this section, we will describe the robust design method that we apply, which is the continuous-time \mathcal{H}_∞ control design with D -scaling.

The generalized plant proposed is depicted in **Fig. 5**, where y and u are the controlled output and control input, respectively. Notice that P is expressed as (1) with parameters given in Table 1. This configuration is intended to evaluate the unstructured model uncertainty as multiplicative error w_1 by the signal z_1 for robust stability and the exogenous disturbance w_2 by the signals z_2 for the disturbance rejection performance. Hence, the

corresponding weighting functions, W_s and W_t , are designed to fit the maximum perturbation model in Fig. 4 and the estimated exogenous disturbance model in Fig. 2, respectively, as shown in those figures. These fitting procedures have been done by using the frequency domain least square fit method with some criteria for their order. The resultant functions have the orders of 9 and 4 for W_s and W_t , respectively.

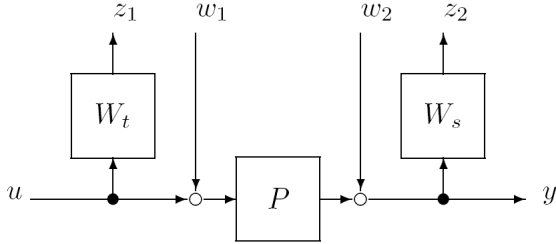


Fig. 5 \mathcal{H}_∞ control problem configuration

Notice that we have taken special consideration on the setting of these weighting functions. Regarding W_s , it is required to have a pole on the origin in order to have the system to be a type 1 servo system, which can reject the biased disturbance. A pseudo integrator $(s + \varepsilon)^{-1}$ is considered here to avoid the computational difficulty¹⁰⁾. The parameter ε is set large enough to make the solution feasible but small enough so that the pseudo integrator becomes an exact one when it is implemented to the actual HDD, of which the onboard MPU/DSP is operated in a fixed point format. Concerning another weighting function W_t , the gain at frequency range higher than the Nyquist frequency is set higher than maximum perturbation model to have a sufficient roll-off. The resultant weighting functions are as follows.

$$\begin{aligned}
 W_s(s) &= \frac{0.132(s+56.33)(s+5386)(s+2580)^2}{(s+1 \times 10^{-5})(s+1956)(s+628)^2(s+130)} \\
 &\quad \frac{(s^2+2.38 \times 10^4 s+2.89 \times 10^8)}{(s^2+2.38 \times 10^4 s+2.90 \times 10^8)} \\
 &\quad \frac{(s^2+1.70 \times 10^4 s+2.88 \times 10^8)}{(s^2+1.51 \times 10^4 s+2.88 \times 10^8)}, \quad (4) \\
 W_t(s) &= \frac{1.90(s^2+3.36 \times 10^4 s+3.72 \times 10^8)}{(s^2+1.95 \times 10^4 s+9.16 \times 10^8)} \\
 &\quad \frac{(s^2+2.42 \times 10^4 s+1.11 \times 10^9)}{(s^2+1.48 \times 10^4 s+1.53 \times 10^9)}.
 \end{aligned}$$

Through the use of the functions above, a desired controller has been obtained by using D-K iteration algorithm¹¹⁾, where a 5th order scaling transfer function is used. Fig. 6 shows the results for $\gamma = 1.192$. The result violates the specification to some extent. However, we may ignore it because of the following reason. The maximum perturbation model is obtained by using the least square fitting technique as in Fig. 4. Because the order of the weighting function should be as low as possible, it

cannot be fit exactly to the maximum multiplicative errors. Consequently, there exists some gap between actual maximum multiplicative errors and the weighting function, which works as a margin. We found that the margin in gain at around the nominal resonant frequency is more than 2dB, thus we concluded that the violation could be ignorable.

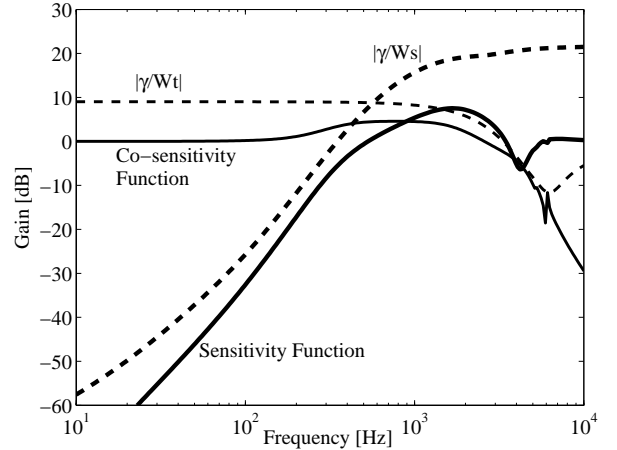


Fig. 6 Specifications and results

The order of the obtained controller was 31, which is not low enough to be implemented on our onboard microprocessor. Here, we use a way of model reduction that considers about the multi-rate implementation (see Appendix A). We obtained a 9th order controller, where the band limited \mathcal{H}_∞ norm of error H_n was 0.12, which is very small and hence ignorable.

4. Frequency division technique (FDT)

In this section, we will explain the basic idea of the proposed frequency division technique (FDT), which includes a temperature dependent filter design and multi-rate digital implementation, and then explain the detailed procedures.

4.1 Basic idea of FDT

The \mathcal{H}_∞ controllers for HDDs can be divided into two parts depending on the frequency of its poles and zeros, i.e., the reduced order controller $K(s)$ represented by

$$K(s) = \frac{\prod_{i=0}^m (c_i s + d_i)}{\prod_{i=0}^n (a_i s + b_i)} \quad (5)$$

can be rewritten as

$$K(s) = K_l(s) \cdot K_h(s) \quad (6)$$

with

$$\begin{aligned}
K_l(s) &= \frac{\prod_{i=0}^{k-1} (c_i s + d_i)}{\prod_{j=0}^{m-1} (a_j s + b_j)}, \\
K_h(s) &= \frac{\prod_{i=k}^n (c_i s + d_i)}{\prod_{i=j}^n (a_i s + b_i)}.
\end{aligned} \tag{7}$$

$K_l(s)$ is a lead-lag type main controller which governs the dominant characteristics in the frequency range within the servo bandwidth, while $K_h(s)$ is normally a notch type filter which compensates the resonant modes in the higher frequency range.

Therefore, a temperature-dependent filter can be designed by manipulating the poles and zeros of $K_h(s)$ by using (3). Detailed discussion will be followed in the next subsection.

On the other hand, in order to have a discrete equivalent of $K(s)$, we have to up-sample the controller, because $K(s)$ tends to have poles and zeros in high frequency region. In this sense, computational saving multi-rate discrete equivalent can be obtained by simply up-sampling only $K_h(s)$. It is because $K_l(s)$ is derived so that it governs low frequency characteristics and does not have to be up-sampled. We will elaborate on it in Subsection 4.3.

Consequently, we can handle two concerns (temperature dependent uncertainty and multi-rate implementation) at the same time by the FDT.

4.2 Temperature dependent filter design

Fig. 7 shows the result of the operation (6) for the nominal temperature case. Notice that, to increase the resolution of appearance, the phase in this figure as well as **Fig. 10** and **Fig. 15** are shown by wrapping up the raw data by 180 degree, which results in the existence of some jumps where the phase crosses the multiple of 180 degree. In this case, the order of $K_h(s)$ is 4, which means it consists of two 2^{nd} order notch filters as we can see from the figure. The transfer functions for these resultant controllers are as follows:

$$\begin{aligned}
K_l(s) &= \frac{0.753(s+254)(s^2+87.2s+6966)}{(s+1 \times 10^{-5})(s+59.7)(s+173.5)(s+786.9)} \\
&\quad \frac{(s^2+2802s+3.77 \times 10^6)}{(s+1.16 \times 10^5)} \\
K_h(s) &= \frac{0.568(s^2+1930s+1.07 \times 10^9)}{(s^2+6918s+7.334 \times 10^8)} \\
&\quad \frac{(s^2+1466s+1.462 \times 10^9)}{(s^2+1356s+1.41 \times 10^9)}
\end{aligned} \tag{8}$$

We now design a temperature dependent filter by modifying the poles and zeros of the filter $K_h(s)$. Although we can design $K_h(s)$ as a function of T_w by using (3), we designed three fixed filters for simplicity that correspond to three fixed temperature zones, namely, low temperature T_L , nominal mid temperature T_M , and high temperature T_H . In other words, we designed $K_h(s, TL)$, $K_h(s, TM)$, $K_h(s, TH)$ instead of $K_h(s, T_w)$. From the nominal case $K_h(s, T_M)$ in (8), we can design

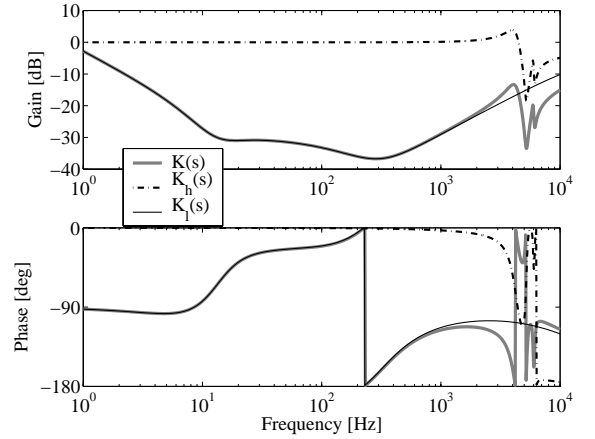


Fig. 7 Result of model division

$K_h(s, TL)$, $K_h(s, TH)$ by modifying the frequency of the poles and zeros of the filters by +5% for the lower temperature zone to have

$$K_h(s, TH) = \frac{0.568(s^2+2026s+1.18 \times 10^9)}{(s^2+7264s+8.09 \times 10^8)} \frac{(s^2+1466s+1.46 \times 10^9)}{(s^2+1356s+1.41 \times 10^9)}, \tag{9}$$

and by -5% for the higher temperature zone to have

$$K_h(s, TL) = \frac{0.568(s^2+1833s+9.69 \times 10^8)}{(s^2+6572s+6.62 \times 10^8)} \frac{(s^2+1466s+1.46 \times 10^9)}{(s^2+1356s+1.41 \times 10^9)}, \tag{10}$$

since the expected temperature fluctuation is around ± 25 degrees-C, that corresponds to around 5% from (3). The configuration of the corresponding control system is depicted in **Fig. 8**.

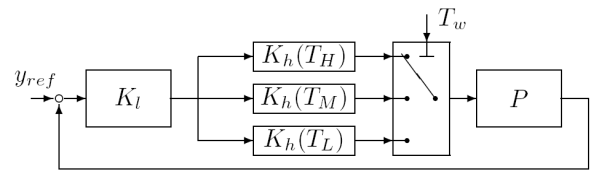


Fig. 8 Feedback system with temperature dependent filter

4.3 Multi-rate implementation

We have divided the original controller into K_l and K_h in the previous subsection. Now, let us introduce a multi-rate scheme as depicted in **Fig. 9**. The control output is first sampled at the original sampling period T_s and is passed through the slow mode compensator K_l to the hold element \mathcal{H}_{T_s} . Then it is re-sampled at the rate of T_s/r to deal with the fast mode filter K_h , where r is a positive integer which denotes the rate of up-sampling. Notice that the up-sampler is followed by a zero-order hold (ZOH) as one of the simplest ways of interpolation to eliminate the imaging component of the spectrum.

In this configuration, K_h is operated at the rate of T_s/r , while K_l is operated at the original sampling period T_s . This means that we can reduce the computational cost when compared to the system where all the filters are operated at T_s/r .

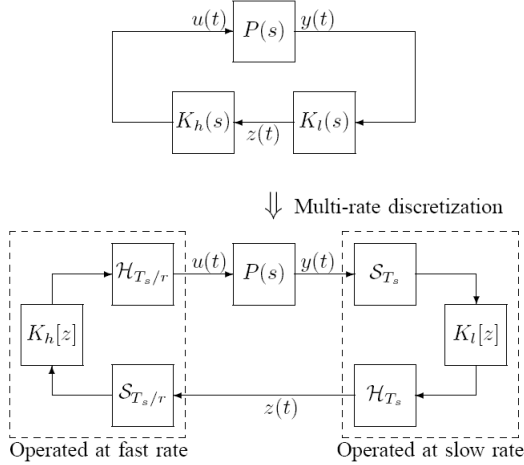


Fig. 9 Block diagram of multi-rate robust control system

All the filters, $K_h(T_H)$, $K_h(T_M)$, $K_h(T_L)$, and K_l , are separately discretized by phase matching method¹²⁾ at the sampling periods of $T_s/2$ and T_s , respectively, i.e., $r = 2$. The resultant controllers are as follows.

$$K_l(z) = \frac{0.0947(z-0.978)(z-0.98)(z-0.996)}{(z-1)(z-0.995)(z-0.985)(z-0.934)} \frac{(z^2-1.76z+0.784)}{(z+0.158)} \quad (11)$$

$$K_h(z) = \frac{0.558(z^2-0.287z+0.943)(z^2+0.1737z+0.963)}{(z^2-0.689z+0.789)(z^2+0.110z+0.965)}$$

where $K_h(z)$ is for T_m .

The frequency response of the original controller $K(s)$ is compared in Fig. 10 to that of the proposed multi-rate controller, which is calculated by deriving its generalized transfer function^{13), 14)}. We can see that the deterioration from the original controller is reasonably small.

Fig. 11 plots the closed-loop frequency responses of the up-sampled system. As can be seen from the figure, the obtained discrete-time system still meets the specifications and is consistent with the continuous-time system (see Fig. 6).

5. Simulations and Experiments

The designed controller is compared to a multi-rate controller without the temperature-dependent filter, which is obtained by considering the thin line instead of bold one in Fig. 4 as the maximum perturbation model for \mathcal{H}_∞ desing.

As we can see from the open-loop frequency responses depicted in Fig. 12, in the standard design, the gain of

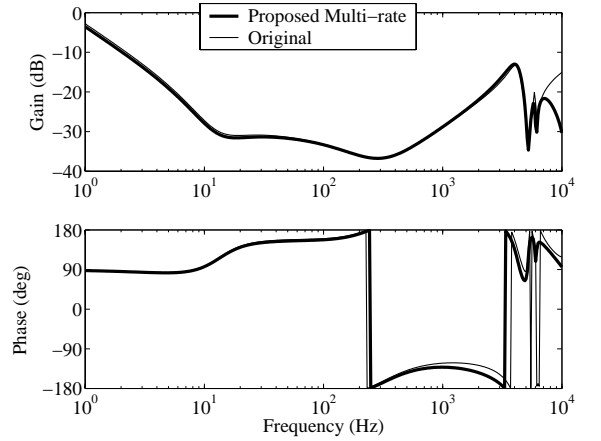


Fig. 10 Comparison of controller frequency responses(sim.)

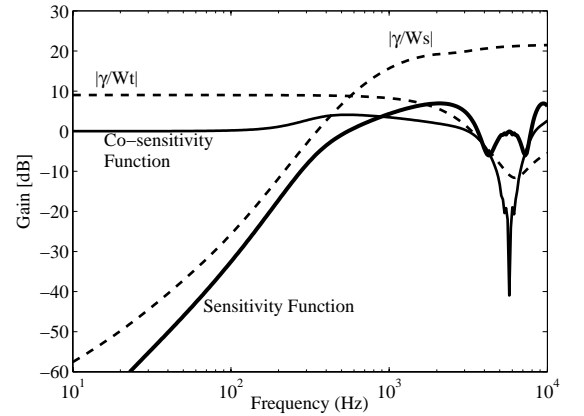


Fig. 11 Specifications and discrete-time results(sim.)

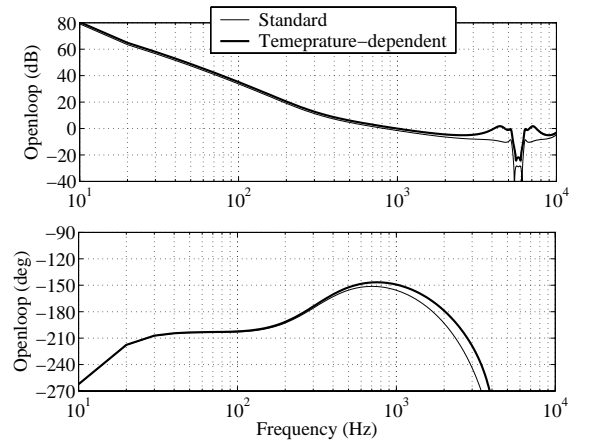


Fig. 12 Comparison of open-loop frequency responses (sim.)

the concerning frequency range of around 5kHz is lowered to accommodate all the possible perturbation, which is depicted as a thin solid line. In contrast with this, our proposed method is aggressively designed in an attempt to obtain the large phase recovery as much as possible. This can greatly affect the disturbance rejection performance in terms of sensitivity function as shown in Fig. 13.

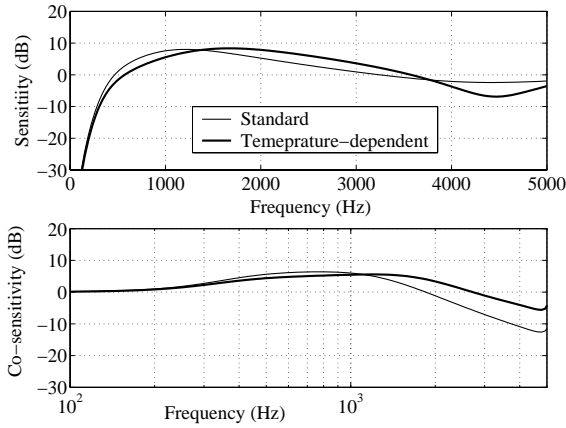


Fig. 13 Comparison of closed-loop frequency responses (sim.)

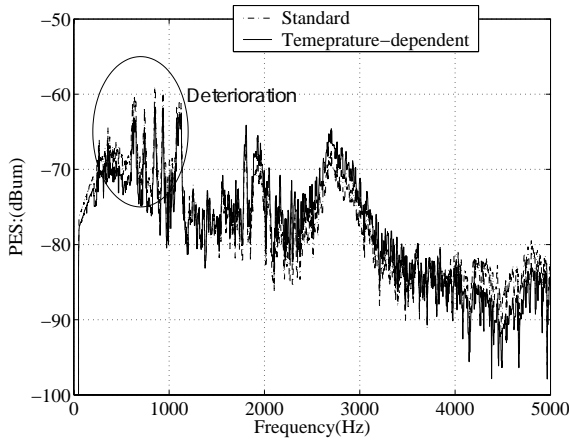


Fig. 14 Comparison of open-loop frequency responses (sim.)

Fig. 14 compares the simulated (estimated) power spectral densities of PESs. As is expected from the sensitivity functions, the PES in the lower frequency range less than 1kHz is much improved, where this range is very important in practice since many mechanical vibrations show up here. By comparing these PESs, we have confirmed that the simulated total NRRO is improved more than 5% by the use of the proposed controller.

We have then conducted experiments using a 3.5", 7,200rpm, 11kHz sampling HDD in order to evaluate the performance of the proposed method.

Fig. 15 and Fig. 16 show the open-loop and closed-loop frequency responses, respectively. We can see from these figures that the designed controller is properly implemented to the experimental setup and the resonant modes around the Nyquist frequency are compensated for as intended. The phase margin and the sensitivity function have been improved compared with the conventional control method, and the bandwidth of the system has been increased at the same time. We can see that the track misregistration has been improved as seen in

Fig. 17 which shows the power spectrum of PES. Notice that the improvement to the conventional one reaches up to 20% at maximum for a specific track and 5% in average for several different units, heads, and tracks.

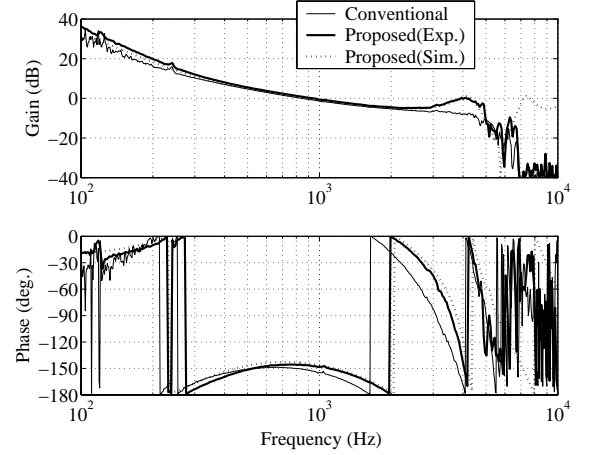


Fig. 15 Open-loop frequency responses (exp.)

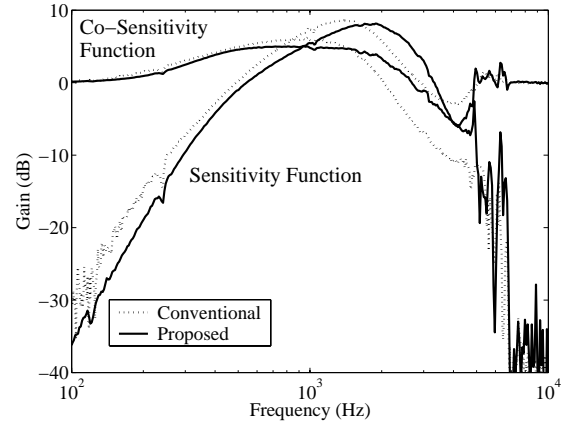


Fig. 16 Closed-loop frequency responses (exp.)

In order to check the compatibility to the seeking control, we have carried out several seek control evaluation experiments.

First, we have introduced a two degree-of-freedom seek control for short track seeking as in ¹⁵⁾, which is to introduce trajectories for both position and control input without changing the feedback controller. We have confirmed that this scheme works well by replacing the conventional feedback controller with our proposed one without modifying anything. An example of a 36-track seek response is illustrated in Fig. 18. Vertical axis stands for the position where a full-scale corresponds to one track, and horizontal one is for time. What is notable is the response marked

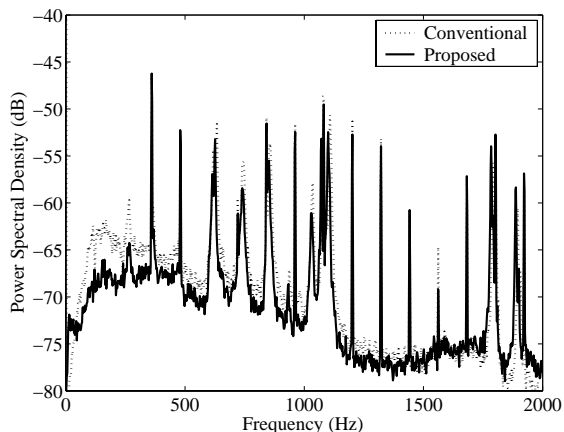


Fig. 17 Power spectral density of PES (exp.)

by an ellipse which corresponds to the one at the last a couple of samples at the end of the seek. From this response, we can see that the position is settled without any residual vibration. Notice that the response except for the one marked by the ellipse looks random because the position measurement resolution of the digital-to-analogue converter is set small.

For longer track seeking control, we utilize the 1st order low-pass filter as a reference filter in conjunction with the IVC¹⁶⁾. Table 3 summarizes the results of 32-track/average-distance seeking for read/write as well as the off-track probability after seeking, which is defined by the number of failures over all seek trials. It shows that no distinctive difference can be found and it can be concluded that the proposed following controller can be implemented successfully from the practical point of view.

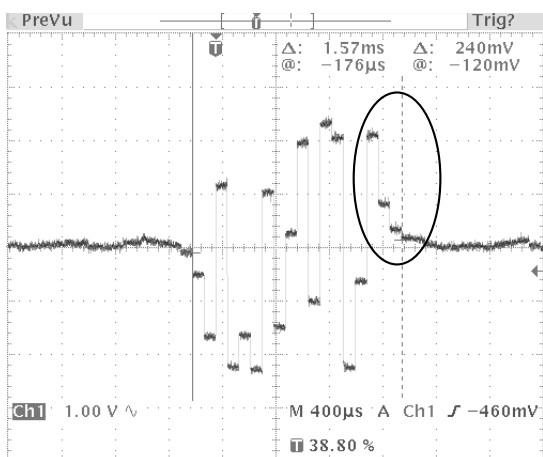


Fig. 18 36-track seek response in time-domain (exp.)

6. Conclusions

We have proposed practical ways of design and imple-

Table 3 Seeking control experimental results

	Conventional	Proposed
32-trk write seek	2.636ms	2.346ms
32-trk read seek	2.219ms	2.170ms
Average-trk write seek	8.812ms	8.971ms
Average-trk read seek	8.364ms	8.367ms
Off-track probability	1.48%	0.80%

mentation of \mathcal{H}_∞ controller for hard disk drive head positioning systems. Introduction of TDUM and FDT make the controller less conservative compared to the standard \mathcal{H}_∞ controllers. The FDT make the controller more computational saving compared to the one when all the modes are operated in high-rate. Also those methods contribute to making the maintenance easier when the resonant characteristics change after design. We have also shown a practical way of combining the proposed controller with a seeking control system.

Several experiments as well as simulations have confirmed the effectiveness by showing that the proposed controller can improve the positioning accuracy by 5% compared to the conventional standard multi-rate controller.

Acknowledgment

This paper is originated from the one presented at the IEEE Conference on Control Applications in 2001 and the authors acknowledge Dr. T. Maruyama at Fujitsu Lab. Ltd. and Mr. T. Hara at Fujitsu Limited for their helpful comments. This research is supported in part by CREST of JST (Japan Science and Technology Agency).

Appendix A. A Controller Order Reduction

A method of model reduction for a certain frequency range based on the least square fit (LSQF)¹¹⁾ is used for controller order reduction. The procedure is given as follows:

- (1) Calculate the band limit ($F_{w1} \sim F_{w2}$) frequency response $K_z := [f \ g]$ of the original controller $K_o(s)$ in a discrete-time sense, where $f \in \mathcal{R}^p$ is a column vector for frequency, $g \in \mathcal{C}^p$ is a column vector for the response, and p is the number of frequency step. [$K_o(s) \rightarrow K_z$]
- (2) Calculate the reduced order model $K(s)$ from the frequency response K_z using the LSQF. [$K_z \rightarrow K(s)$]
- (3) Calculate the multiplicative (or additive) error $W_z(s)$ between the reduced order model $K(s)$ and the original one $K_o(s)$. [$K_o(s), K(s) \rightarrow W_z(s)$]
- (4) Calculate the band limit ($F_{w1} \sim F_{w2}$) \mathcal{H}_∞ norm $H_n \in \mathcal{R}$ of $W_z(s)$. [$W_z(s) \rightarrow H_n$]
- (5) Let $W_z(s)$ be a weight for the next LSQF and iterate from Step 1 to Step 4 several times.

(6) Iterate from step 1 to Step 5 and find the minimum H_n . Corresponding $K(s)$ is to be the reduced order controller.

We set F_{w1} as 0 and F_{w2} as the sampling frequency F_s because we will deal with the $2 \times$ multi-rate system in this paper, and F_s is the Nyquist frequency of the fastest rate $2F_s$ of the system.

Appendix References

- 1) M. Hirata, K. Z. Liu, T. Mita and T. Yamaguchi: Head positioning control of a hard disk drive using H_∞ theory, In 31st IEEE Conference on Decision and Control, **2**, 2460/2461 (1992)
- 2) S. Hara, M. Nishio and T. Maruyama: Integrated Design for High Robust Performance with Quick Time-Response, Proceedings of the International Conference on Control Applications, 176/181 (1999)
- 3) T. Semba: An H_∞ Design Method for a Multi-Rate Servo Controller and Applications to a High Density Hard Disk Drive, Proc. of the 40th IEEE Conference on Decision and Control, 4693/4698 (2001)
- 4) M. Takiguchi, M. Hirata and K. Nonami: Following Control of Hard Disk Drives Using Multi-rate H_∞ Control, Proc. of SICE Annual Conference (2002)
- 5) M. Hirata, T. Atsumi, A. Murase and K. Nonami: Following Control of a Hard Disk Drive by using Sampled-Data H_∞ Control, In Proc. of the 1999 IEEE International Conference on Control Applications, 182/186 (1999)
- 6) S. C. Wu and M. Tomizuka: Multi-rate digital control with interlacing and its application to hard disk drive servo, Proc. of the American Control Conference, 4347/4352 (2003)
- 7) G. F. Franklin, J. D. Powell and M. Workman: Digital Control of Dynamic Systems-Third Edition, Addison Wesley (1998)
- 8) M. Banther, Y. Huang and W.C. Messner: Optimal strain gauge placement for an instrumented disk drive suspension, Proc. American Control Conf., 3023/3027 (1998)
- 9) R. L. Burden and J. D. Faires: Numerical Analysis Seventh Edition, Brooks Cole (2001)
- 10) K. Nonami, H. Nishimura and M. Hirata: Control System Design Using MATLAB, Tokyo Denki Publishing (1998)
- 11) G. J. Balas, J. C. Doyle, K. Glover, A. Packard and R. Smith: μ -Analysis and Synthesis Toolbox for use with MATLAB, The Mathworks, version 3 (2001)
- 12) H. Yamaura and M. Tomizuka: A New Design Method for Discrete Equivalents of Analog Controllers, Proceedings of the American Control Conference, 1986/1992 (2000)
- 13) S. Wu and M. Tomizuka: Performance and Aliasing Analysis of Multi-rate Digital Controllers with Interlacing, proc. of the American Control Conference, 3514/3519, Boston (2004)
- 14) R. A. Meyer and C. S. Burrus: A Unified Analysis of Multirate and Periodically Time-Varying Digital Filters, IEEE Trans. on Circuits and Systems, **CAS-22-3** (1975)
- 15) K. Takaishi: Fast Seek Control Taming Actuator Vibration for Magnetic Disk Drive, INTERMAG'99, **FS-14** (1999)
- 16) T. Yamaguchi, K. Shishida, S. Tohyama and H. Hirai: Mode switching control design with initial value compensation and its application to head positioning control on magnetic disk drives, IEEE Transactions on Industrial Electronics, **43-1**, 65/73 (1996)

Keitaro OHNO (Member)



Keitaro Ohno received B.S. and M.S. degrees in mechanical engineering from Tokyo Institute of Technology in 1991 and 1993, respectively. From 1993 to 1999, he was with the Space Development Group, Fujitsu Limited. In 1999, he joined the Autonomous System Laboratory in Fujitsu Laboratories Limited. From 2001 to 2003, he was a visiting industrial fellow at the Computer Mechanics Laboratory in the University of California at Berkeley. He served as a private secretary to the Minister of State from 2004 to 2005, and then, as a policy staff to a member of the House of Representatives. Since 2006, he has been with the Department of Information Physics and Computing of the University of Tokyo. His research interest includes robust and optimal control in robotics and HDD servos. He is a member of ASME, and IEEE.

Shinji HARA (Member)



Shinji Hara received the B.S., M.S., and Ph.D. degrees in engineering from Tokyo Institute of Technology, Tokyo, Japan, in 1974, 1976 and 1981, respectively. From 1976 to 1980 he was a Research Member of Nippon Telegraph and Telephone Public Corporation, Japan. He served as Research Associate at the Technological University of Nagaoka from 1980 to 1984. In 1984 he joined Tokyo Institute of Technology as an Associate Professor and had served as a Full Professor ten years. Since 2001 he has been a Full Professor of Department of Information Physics and Computing, The University of Tokyo. He received Best Paper Awards from SICE (the Society of Instrument and Control Engineers, Japan) in 1987, 1991, 1992, 1997 and 1998, from Japan Society for Simulation Technology in 2001, and from ISCIE in 2002. His current research interests are in robust control, sampled-data control, hybrid control, learning control, quantum control and computational aspects of control system design. Dr. Hara is a fellow of IEEE. He was a BoG member of IEEE Control System Society, the General Chair of the CCA04, and an Associate Editor of IEEE Transactions on Automatic Control and Automatica.
